To be submitted to Journal of Power Sources

# SSH2S: hydrogen storage in complex hydrides for an auxiliary power unit based on high temperature proton exchange membrane fuel cells

*Marcello Baricco*[a], *Mads Bang*[b], *Maximilian Fichtner*[c], *Bjorn Hauback*[d], *Marc Linder*[e], *Carlo Luetto*[f], *Pietro Moretto*[g], *Mauro Sgroi*[h*]

[a] Department of Chemistry and NIS, University of Turin, via P.Giuria 7, I-10125 Torino, Italy

[b] Serenergy A/S, Lyngvej 8, 9000 Aalborg, Denmark

[c] Karlsruhe Institute of Technology, Institute of Nanotechnology, Hermann-von-Helmholtz Platz 1, D-76344 Eggenstein-Leopoldshafen

[d] Physics Department, Institute for Energy Technology, P.O. Box 40, NO-2027 Kjeller, Norway

[e] Institute of Engineering Thermodynamics, German Aerospace Center (DLR), Pfaffenwaldring 38-40, 70569 Stuttgart, Germany

[f] Tecnodelta s.r.l.- Via F.Parigi 5/H – 10034 Chivasso (TO), Italy

[g] European Commission, Joint Research Centre (JRC), Directorate for Energy, Transport and Climate, Westerduinweg 3, NL-1755 LE Petten, The Netherlands

[h] Centro Ricerche Fiat S.C.p.A., Strada Torino 50, 10043 Orbassano (TO), Italy

**Abstract**

The main objective of the SSH2S (Fuel Cell Coupled Solid State Hydrogen Storage Tank) project was to develop a solid state hydrogen storage tank based on complex hydrides and to fully integrate it with a High Temperature Proton Exchange Membrane (HT-PEM) fuel cell stack. A mixed lithium amide/magnesium hydride system was used as the main storage material for the tank, due to its high gravimetric storage capacity and relatively low hydrogen desorption temperature. The mixed

lithium amide/magnesium hydride system was coupled with a standard intermetallic compound to take advantage of its capability to release hydrogen at ambient temperature and to ensure a fast start-up of the system. The hydrogen storage tank was designed to feed a 1 kW HT-PEM stack for 2 hours to be used for an Auxiliary Power Unit (APU). A full thermal integration was possible thanks to the high operation temperature of the fuel cell and to the relative low temperature (170 °C) for hydrogen release from the mixed lithium amide/magnesium hydride system.

**Keywords:** Hydrogen storage, high temperature fuel cell, Auxiliary Power Unit, lithium amide, magnesium hydride.

* corresponding author:

Dr. Mauro Francesco Sgroi
Group Materials Labs
Centro Ricerche FIAT S.C.p.A.
Strada Torino, 50
10043 Orbassano (TO), Italy
Tel. + 39 011 9083552
Fax. + 39 011 9083666
e-mail: mauro.sgroi@crf.it

## 1 Introduction

In this paper, we report the results of the SSH2S (Fuel Cell Coupled Solid State Hydrogen Storage Tank) project [1], aimed to develop a hydrogen fuelled Auxiliary Power Unit (APU) to be installed on a light duty commercial vehicle. A prototype hydrogen storage tank based on hydrides was developed and it was thermally coupled with a high temperature polymeric fuel cell stack, operating between 160 °C and 180 °C. The project was supported by the European Fuel Cells and Hydrogen Joint Undertaking (FCH-JU).

Fuel cell-based APUs were intensively studied during the last years for application on diesel fuelled heavy and light duty commercial vehicles, with the aim to reduce the noxious and polluting emissions related the engine idling used to power auxiliary systems (such as air-conditioning) during the parking of the vehicle [2–4]. For this reason, the majority of the suggested alternative systems was based on a processor able to produce hydrogen from the diesel fuel already present on-board and to deliver it to a polymeric fuel cell stack [5, 6]. Some efforts have been devoted to the processing of biodiesel fuel to be used as a renewable fuel and to reduce the carbon footprint of the technology [7, 8]. The hydrogen produced from diesel fuel requires purification before use, especially from carbon monoxide (CO) and hydrogen sulphide ($H_2S$), which can poison the anodic catalysts of the fuel cell. The required quality of hydrogen is directly connected with the cost and weight of the fuel processor: reaching hydrogen purity grade for fuel cell can be not practical or not economically convenient for automotive applications. For this reason, recent works proposed the use of high-temperature fuel cell stacks, since at temperature in the range 150-180 °C the fuel cell catalyst is more tolerant to CO impurities [9, 10].

It is worth to mention that on-board hydrogen production is not a completely a zero emission approach, since the fuel processor produces a small amount of $CO_2$. An alternative approach, having the advantage of not producing local emissions, is on-board hydrogen storage. The most mature and widely applied technology is compressed hydrogen, which requires the availability of a

high pressure refuelling infrastructure. The automotive applications are currently adopting two standard pressures of 35 and 70 MPa. It can be expected that fast refill of small tanks, such as the ones required for APU fuelling, will not be fully compatible with the mentioned infrastructure for vehicles. For this reason, it is worth to investigate solutions which would allow storing hydrogen at lower pressures, which can be easy achieved by simple and inexpensive pressure boosters. This approach has the additional advantage to reduce the cost of compression and to avoid preventive actions required to guarantee the safety of the storage system. Solid state hydrogen storage is characterized by relatively low operating pressures, and it has been the subject of many investigations in the recent years [11–17].

Well known materials for hydrogen storage, showing very stable performances and acceptable reversibility of hydrogen sorption reaction, belong to the class of interstitial metal hydrides (MeH) [15], characterized by gravimetric capacities lower than 2 wt% $H_2$. Early investigated examples are TiFe and $LaNi_5$ compounds. Complex hydrides (CxH) [16–18] have attracted considerable attentions in the past years due to their high $H_2$ capacities, compared to metal hydrides. These compounds have the general formula $M_xM'_yH_n$, where M is an alkali metal cation and M' is a metal or metalloid. Common examples include sodium and lithium alanate ($NaAlH_4$ and $LiAlH_4$) and lithium borohydride ($LiBH_4$). The first integration of hydrogen storage system, based on complex hydride, with an high temperature fuel cell stack was reported by Fichtner et al. [19].Considering materials based on complex hydrides, Li-Mg-N-H system, consisting of $Mg(NH_2)_2$ and LiH, possesses good reversibility and hydrogen sorption properties, as well as relatively low operation temperatures (< 200 °C) [19, 20]. A mixture of $LiNH_2$ and $MgH_2$ is regarded as the equivalent system to the $Mg(NH_2)_2$-LiH combination, because of the following metathesis reaction between the two metal hydride-amide pairs [22]:

$$2\ LiNH_2 + MgH_2 \rightarrow Mg(NH_2)_2 + 2\ LiH \quad (1)$$

Experimental results showed that the combination of $Mg(NH_2)_2$-LiH is thermodynamically more stable. Therefore, after a cycle of hydrogen desorption and re-hydrogenation, the system becomes *de facto* a $Mg(NH_2)_2$-LiH mixture [23]. Recently, it was shown that Li-Mg-N-H system can be catalysed by mixed transition metal compounds, which enable a reversible hydrogen storage capacity of about 4.5 wt% $H_2$ at temperatures below 200 °C [23, 24]. For this reason the effect of different additives was investigated in this work and the $2LiNH_2$ - $1.1MgH_2$ - $0.1LiBH_4$ - 3wt% $ZrCoH_3$ system [26] was finally selected as active material for the solid state hydrogen storage tank. Hydrogen desorption reaction brings to the formation of a mixed imide with chemical formula $Li_2MgN_2H_2$, together with some residual $ZrCoH_3$, corresponding to a hydrogen release of 4.5 wt% $H_2$ in about 300 min under 0.1 MPa at 150 °C. Hydrogen absorption of 5.3 wt% $H_2$ has been obtained in about 20 min under 7.0 MPa at 150 °C. Reversibility of hydrogen sorption reactions has been demonstrated for this system up to 10 cycles [26]. Further studies extended the analysis up to 30 cycles, showing partial reduction of the hydrogen gravimetric density [27].

Moreover, a new concept of thermal coupling of the mixed lithium amide/magnesium hydride system with an intermetallic compound, $LaNi_{4.3}Al_{0.4}Mn_{0.3}$, was investigated. The idea is to exploit a synergic combination of advantages from both materials: MeH, even if characterized by low gravimetric hydrogen storage capacity, has fast hydrogen sorption kinetics at room temperature, whereas the CxH has higher hydrogen storage capacity, but shows slow reaction rates at low temperatures. The goal is therefore to combine both materials in the tank, leading to an increase of temperature at the beginning of the hydrogen sorption process, because of the heat released by hydrogen absorption in MeH, facilitating the first hydrogen uptake by the CxH. As soon as this part of the CxH is active, its exothermic hydrogen absorption will lead to a temperature increases in the whole tank, leading to an accelerated hydrogen uptake.

In this paper, the main activities performed in the frame of the SSH2S project will be reported, showing the progress toward the implementation of a solid state hydrogen tank based on a mixed

lithium amide/magnesium hydride system, to be coupled with a high temperature fuel cell powering a 1 kWh APU, installed in a light duty commercial vehicle.

## 2 Methodology

### 2.1 Materials preparation and characterization

The complex hydride based system (CxH), catalysed with different additives, was produced using high-energy ball milling. $LiNH_2$ (from Sigma Aldrich, purity >95%), $MgH_2$ (Alfa Aesar, purity 98%) and $LiBH_4$ (Alfa Aesar, purity 95%) were stored in a glove-box under Ar as protecting atmosphere and used as-received. KH suspension (Alfa Aesar, purity 35 % in protective oil) was filtered, washed with dry hexane and dried with a Büchi rotation evaporator. ZrCo ingots were supplied by SAES Getters S.p.A. (Italy) and converted to $ZrCoH_3$ by interaction with hydrogen at 1 MPa $H_2$ pressure and ambient temperature. For the ball milling process, the starting chemicals were loaded into a milling vessel inside the glove-box. A Retsch PM 400E mill was used for screening the effect of the additives. As MeH material, $LaNi_{4.3}Al_{0.4}Mn_{0.3}$ has been used, because the equilibrium pressure of this material at room temperature is below the equilibrium pressure for the Li-Mg-N-H system. The material has been obtained from Konik Industries Corporation, Shenzhen, Guangdong (China).

A carefully calibrated home-made Sieverts' system was used to measure $H_2$ evolution in a Temperature Programmed Desorption (TPD) in isothermal desorption mode, under 0.1 MPa of hydrogen. For the desorption isotherms, the temperature was first raised to 180 °C at 5 °C $min^{-1}$ and held constant for 140 minutes. Absorption and desorption Pressure-Composition-Temperature (PCT) measurements were performed using a volumetric instrument (Advanced Materials Corporation, Pittsburgh). Equilibrium profiles were generated at different isotherms up to 200 °C and by applying pressures in steps up to 100 bar $H_2$.

The composition of gas desorbed from the mixed lithium amide/magnesium hydride system was analysed coupling the TPD apparatus with a MKS Microvision-IP Rest Gas Analyser mass

spectrometer (MS). The possible chemical interaction between the complex and the metal hydrides was investigated by scanning electron microscopy (SEM, Zeiss SUPRA 50) and X-ray energy dispersion spectroscopy (EDS, Oxford Inca).

### 2.2 Finite elements modelling and storage system testing

The storage vessel was modelled using 2D computational fluid dynamics (CFD) simulations based on the finite elements method [28] and performed with the commercial COMSOL code [29]. The model included heat and mass transfer, pressure drop as well as absorption and desorption reactions. Moreover, the model was extended to include the combination of the intermetallic compound with the complex hydride: this allowed investigating if the heat of reaction provided by MeH is rapidly transferred to lead to the desired temperature increase of the CxH and helped to understand the role of the reactor geometry on these self-accelerating hydrogen sorption processes [30].

The simulation results (see section 3.2) showed that to improve the heat transport between the storing materials and the fluid used for the heat exchange the storage system has to be composed by twelve cylindrical vessels connected in parallel. After the design guided by finite elements modelling, the storage system was built using stainless steel tubes welded using the Tungsten Inert Gas (TIG) technique. To avoid contact between the hydrogen storage material and air, a custom glove-box was built for the fabrication of the vessels.

The storage system was tested by a custom experimental set-up able to simulate real charge/discharge processes: hydrogen pressures up to 150 bar have been applied and the heat transfer fuel flow has been controlled at temperatures up to 200 °C. Each storage vessel was equipped with a temperature sensor. Hydrogen was supplied or released by pressure or mass-flow control up to 20 $Nl \cdot min^{-1}$: this flow rate was not sufficient to perform fast charging tests on the complete system. For this reason, a single vessel was filled at high flow rate demonstrating the possibility to completely fill the hydrogen storing materials in 15 minutes. For desorption

experiments, the boundary conditions were set-up according to the foreseen coupling with the fuel cell stack.

## 3 Results and discussion

### 3.1 Material selection for hydrogen storage

In order to select the material to be used for the hydrogen tank, a mixture based on $2LiNH_2$-$1.1MgH_2$ was ball-milled with different additives (i.e. $LiBH_4$, KH and $ZrCoH_3$) to obtain the various mixtures. The effect of different additives on hydrogen desorption was studied using TPD at 180 °C and the results are shown in *Figure 1*.

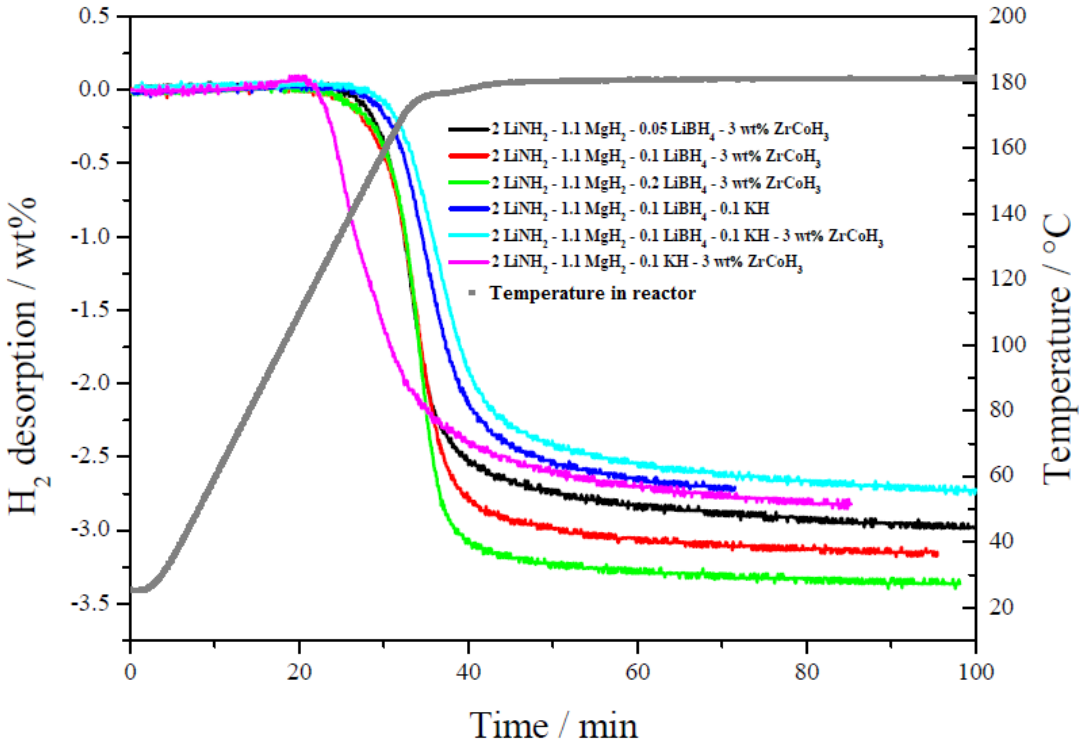


*Figure 1: Hydrogen desorption isotherms under 0.1 MPa of hydrogen for the 2 $LiNH_2$ – 1.1 $MgH_2$ systems with and without addition of $LiBH_4$, $ZrCoH_3$ and KH in varying amounts.*

On the basis of the gravimetric capacity and desorption kinetics, as well as the stability to hydrogen absorption/desorption cycles [31], the $2LiNH_2$ - $1.1MgH_2$ - $0.1LiBH_4$ - 3wt% $ZrCoH_3$ mixture was selected for building the storage system. After an activation pre-treatment of the sample with three

cycles of absorption at 100 bar / desorption in vacuum at 150 °C, PCT measurements were performed. In order to obtain equilibrium data, various cycles of hydrogen absorption and desorption have been carried out. The results obtained for the first desorption are reported in Figure 2. It turns out that, at 150 °C, equilibrium conditions cannot be reached because of kinetic constraints, so that a limited amount of hydrogen can be desorbed (i.e. 2 wt% $H_2$). For higher temperatures, equilibrium conditions can be easily obtained, leading to hydrogen desorption of about 4.0-4.5 wt% $H_2$, so that a plateau pressure can be identified. From the analysis of the equilibrium pressure at various temperatures, the desorption enthalpy of the system was determined to be -45 $kJ \cdot mol_{H2}^{-1}$ [30]. Data shown in *Figure 1* and *Figure 2* confirm that the selected mixture is suitable to be coupled with a HT-PEM fuel cell.

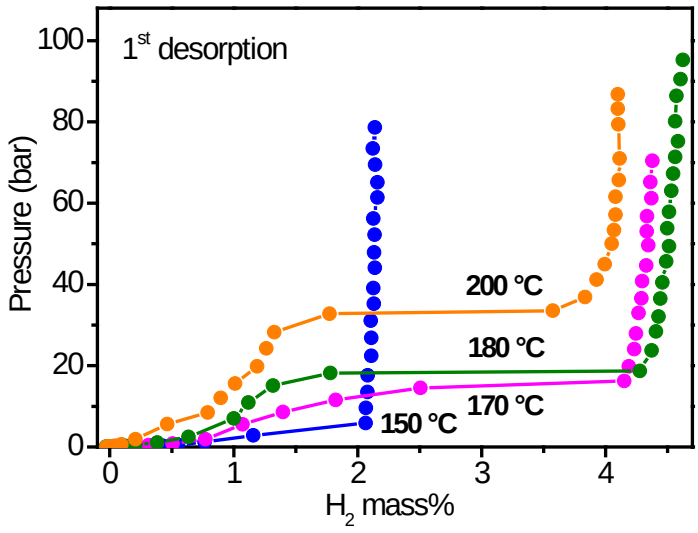


*Figure 2:PCT curves (1st desorption, after activation) of the $2LiNH_2$ - $1.1MgH_2$ - $0.1LiBH_4$ - $3wt\%\ ZrCoH_3$ system. Temperatures are indicated in the figure.*

The ball milling procedure was optimized to obtain good cycle stability and reversibility in the hydrogen sorption test. Hydrogen absorption and desorption reaction rates were established [30], indicating that more than 70% of hydrogen can be released at 160 °C in about 1 hour. Considering the whole set of data obtained for the characterisation of hydrogen sorption reactions, the optimal

operating temperature combing desirable kinetics, full reversibility and good storage capacity was selected at 160 °C. TPD-MS analysis in the temperature region of 25 - 600 °C showed that the mass loss up to 220 °C can be attributed merely to hydrogen evolution. In fact, signals related to masses 26 and 27, due to release of B – H species were 100 times smaller than that of the mass 2, due to hydrogen delivery. Similarly, signals of masses 12, 14 or 17, related to delivering of N – H species, were 2 orders of magnitude lower than that due to mass 2. So the di-borane or ammonia emissions were negligible, confirming the absence of gaseous species which can poison the catalyst of the anodes of the fuel cell stack.

The use of a direct mixture of MeH ($LaNi_{4.3}Al_{0.4}Mn_{0.3}$) with the selected CxH system as active material was investigated as a first option. However, the mixture exhibited a rapid decrement of storage capacity upon cycling. X-ray energy dispersion spectroscopy (EDS) identified in the mixture a La-Ni-Mg containing phase, suggesting chemical interaction between the mixed lithium amide/magnesium hydride system and the intermetallic material. For this reason, the two materials were kept separated, but in thermal contact, in the hydrogen storage tank.

### 3.2 Development and testing of the hydrogen storage system

The storage system was conceived exploiting a new concept of thermal coupling of the complex and metal hydrides. This solution combines the advantages of both materials and facilitates the charging process: during the first phase of hydrogen absorption, at ambient temperature, the heat released by the MeH helps to enhance the temperature of the reacting bed up to 100 °C, when also the CxH system can start the hydrogen uptake. Moreover, during desorption, the fast desorption kinetics of MeH can help to sustain transitory peak requests of hydrogen from the fuel cell stack.

The tank design process was guided by CFD simulations of the behaviour of the storing materials inside of the tank. The tank geometry used for simulation is shown in *Figure 3* (left and middle). It basically consists of two separate concentric cylindrical compartments containing, respectively, MeH and CxH (combi-tank concept) that are separated by a filter mesh made of copper. The

cylindrical symmetry of the problem allows reducing the computational effort by selecting the computational domain depicted in red in *Figure 3* (left). Results of the 2D simulation provided the temperature evolution in the tank as a function of time. As an example, the temperature distribution at the point in time shortly before the CxH starts to absorb is reported in *Figure 3* (right). One of the main advantages of the combi-tank concept is indicated by the red arrow: due to the internal heat generation by the exothermic reaction of MeH, a heat flux is triggered from the centre to the outer cooling surface. Consequently, an external heating of the CxH at the beginning is not required and towards the end of the reaction the required cooling load is clearly reduced.

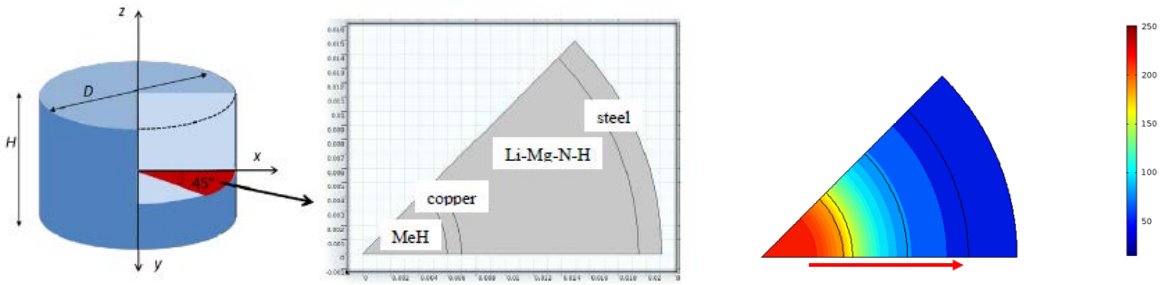


*Figure 3: Left and middle: tank geometry used for simulation. Right: results of 2D simulation at the point in time shortly before the CxH starts to absorb and increases its temperature. The red arrow indicates the direction of heat flux. The bar indicated the temperature scale.*

The simulation results suggested how to improve the heat exchange to and from the reacting bed, how to reduce the thermal inertia of the system and the start-up time for hydrogen desorption. These goals can be achieved distributing the storing phase in multiple small vessels connected in parallel instead of using a single big tank containing all the required storage material. Moreover, the best CxH:MeH gravimetric ratio for optimizing the kinetics of absorption and desorption has been calculated to be equal to 1:1. The complete results of finite elements simulations were published

elsewhere [32–34]. On the basis of that complete study, the geometry of the single storage vessel was defined: each container is built using stainless steel and comprises two concentric cylindrical compartments containing the MeH (inner shell) and the CxH (outer shell), as shown in *Figure 4a*. The two materials compartments were separated by a porous medium with a 0.2 mm porosity, to avoid mixing but allowing the fast flowing of hydrogen and the heat exchange. The heating and cooling system consisted in a jacket surrounding each single vessel in which thermal fluid, used to couple the storage tank with the high temperature fuel cell stack, was circulated.

The scale-up for the material production was performed on a vibrational ball-mill by Siebtechnik GmbH, housed in a nitrogen filled glove-box. The mixed lithium amide/magnesium hydride system to be used for the tank was prepared with a ball to powder ratio of 390:1 at 1200 rpm of the eccentric drive, 2000 steel balls with a diameter of 20 mm and a total milling time of 5 hours. In total, the tank was filled with 3.4 kg of metal hydride and 3.4 kg of Li-Mg-N-H mixture. Twelve single vessels were assembled in parallel, as shown in *Figure 4b*. A thermocouple was inserted in each single vessel in order to monitor the temperature during operation. Overall dimensions of the tank are reported in *Figure 4*c, together with details of connections and valves.

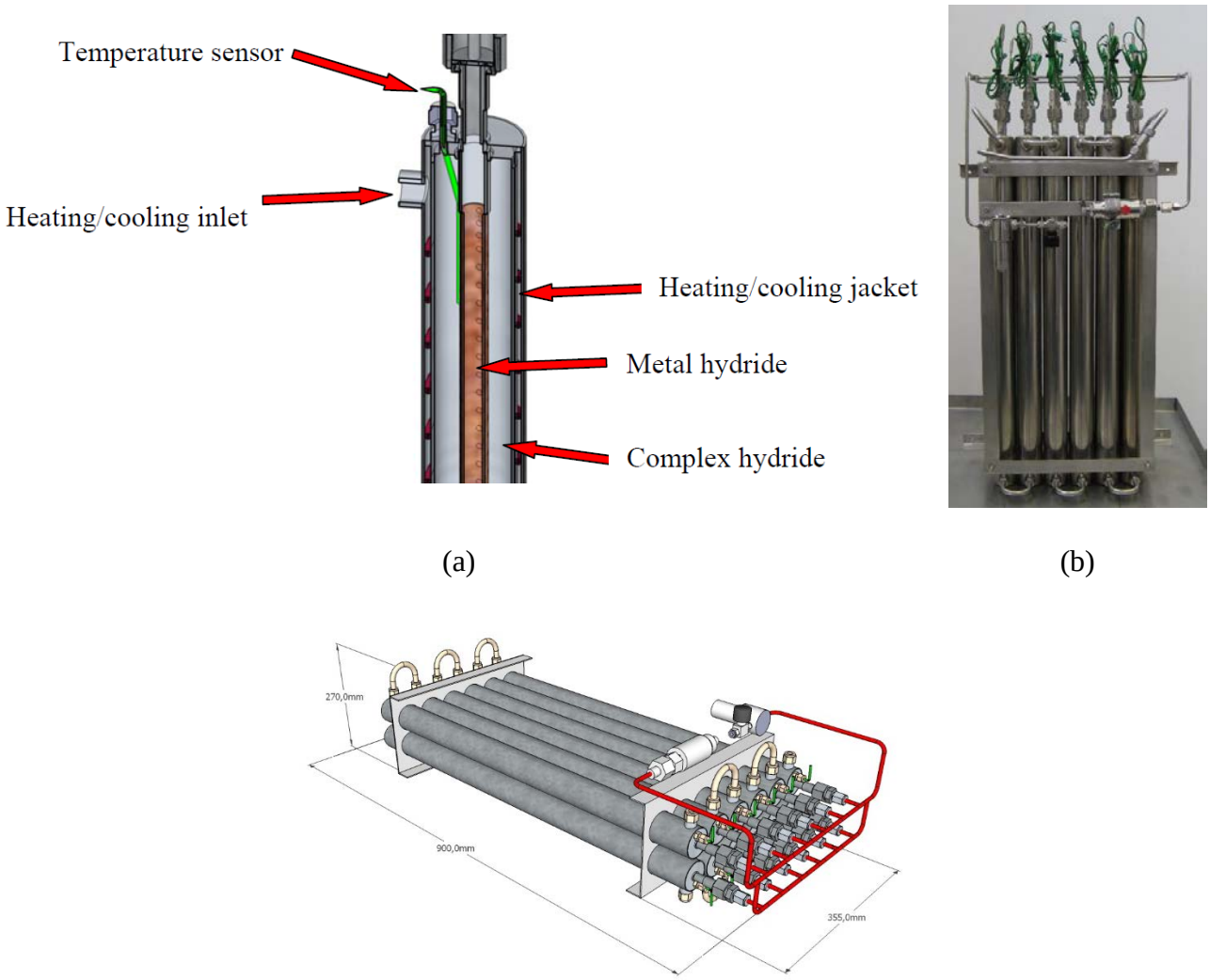


*Figure 4: a) Scheme of single vessel implementing the double storage materials concept (combi-tank); b) assembly of twelve vessels in parallel to form the complete storage system; c) overall dimensions of the system.*

The storage tank was characterized using the custom test bench before the integration with the fuel cell system. The hydrogen filling pressure was 67 bar, in order to guarantee the complete charging of the tank (in accordance with PCT measurements reported in *Figure 2*). Hydrogen was then released at constant mass flow rate. As soon as the pressure reached a value lower than the equilibrium pressure of the system, the material started to desorb and a plateau in pressure vs time

was reached. During the experiment, the temperature of the heat transfer fluid was kept constant at 180 °C (corresponding to the operating temperature of the HT-PEM fuel cell) and the minimum final pressure was set to 1.7 bar, a value compatible with the pressure drop encountered in the hydrogen inlet line of the fuel cell stack.

The time dependence of pressure during hydrogen desorption from one single tube at different hydrogen flow rates is reported in *Figure 5*. As expected, the pressure drops until it reaches a pressure at which the endothermic release of hydrogen starts. It is interesting to note that this plateau of the pressure signal depends on the adjusted flow rate. Since the higher flow rates the more thermal energy is required, the temperature gradient between the heat transfer fluid and the reaction temperature has to increase for high discharge rates, so that the pressure of released hydrogen is reduced. Taking into account that the final prototype was built of 12 identical tubes, it can operate at nominal power ($1 Nl \cdot min^{-1}$) with an efficiency of 45 % for around 2 hours until the pressure drops below the required value (1.7 bar). Additionally, it can be stated that the storage system is able to supply the fuel cell stack for more than 4 h at 50 % load.

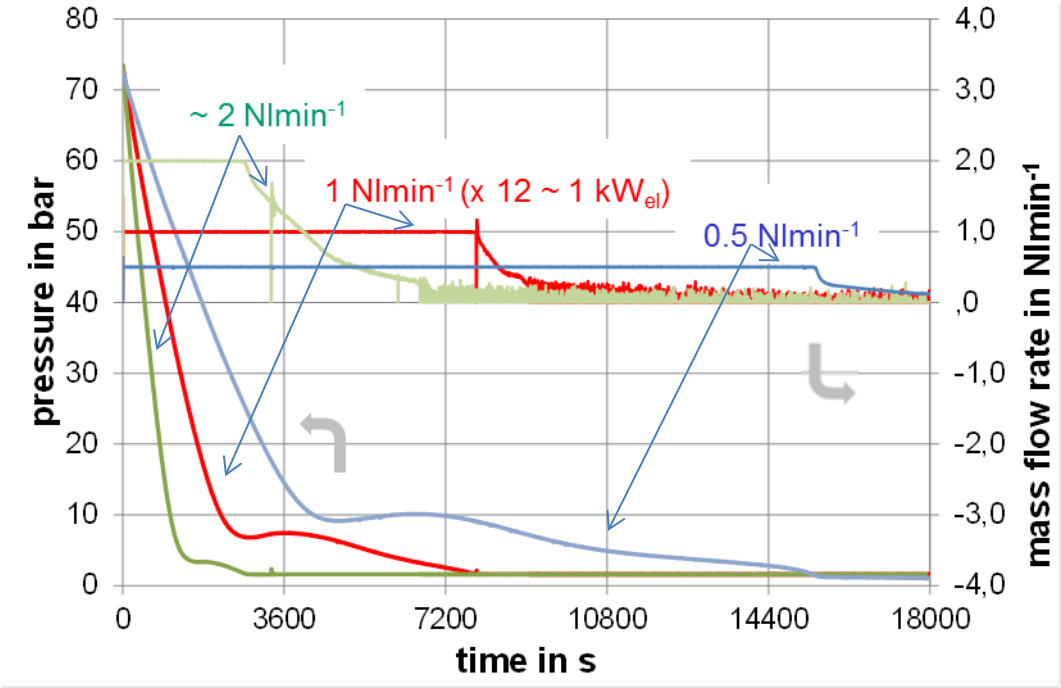


*Figure 5: Hydrogen desorption from one single tube at 180 °C. Flow rates (right side) and corresponding pressure (left side) are shown as a function of time. Final tank consists of 12 similar tubes operated in parallel.*

The overall hydrogen amount released by the tank has been calculated integrating the mass flow rate over time interval of two hours and it was determined to be 173 g. Since 6 g of hydrogen were stored as gaseous phase in the free volume of the prototype tank, a mass of about 167 g of hydrogen has been estimated to be stored in the solid phases. This value corresponds to a gravimetric hydrogen storage density of 2.45 wt% $H_2$ for the combined materials. The volumetric storage capacity of the tank is 10 $g \cdot l^{-1}$, to be compared with compressed hydrogen tanks, which ranges between 9 $g \cdot l^{-1}$ and 23 $g \cdot l^{-1}$ for steel cylinders at 200 bar and type IV composite cylinders at 700 bar, respectively [35]. On the other hand, liquid hydrogen based storage systems can reach a volumetric capacity of 40 $g \cdot l^{-1}$, but suffer from an extremely complex thermal management and from the continuous hydrogen boil-off [35].

### 3.3 APU building and system testing

The developed solid state hydrogen tank was thermally coupled with a liquid cooled HT-PEM fuel cell stack to build the APU. The operating principle of the system is based on using the heat released by the fuel cell stack to desorb hydrogen from the solid state hydrogen storage tank. This was possible thanks to the high operation temperature of the fuel cell and to the relatively low hydrogen desorption temperature of the developed hydrogen storage materials. It is worth noting that this approach allows recovering part of the heat released by the fuel cell stack, whereas in APU systems employing compressed hydrogen it has to be dissipated to the ambient. The design specifications of the APU, based on the requirements for the installation on a light duty commercial vehicle, are reported in *Table 1*.

*Table 1: Specifications of the 1kW APU.*

| | |
|---|---|
| Operating time | 2h |
| Total stored energy | 5 kWh |
| Fuel cell efficiency | 0.4 |
| $H_2$ storage capacity | 1400 Nl |
| Maximum $H_2$ internal pressure | 100 bar |
| Maximum temperature | 200 °C |
| Maximum $H_2$ release pressure | 1.5 bar |
| Average $H_2$ flow rate to the fuel cell | 20 Nl·min$^{-1}$ |
| Maximum filling time | 15 min |

A 1 kW HT-PEM fuel cell stack, based on polybenzimidazole/phosphoric acid membranes, was supplied by Serenergy A/S. The cathode of the fuel cell system was fed by a blower with filtered air from environment. Temperature and mass flow were monitored at stack inlet. At cathode side, only the temperature of the waste gas was monitored, to ensure that no condensate droplets could return back to the stack. So, a solenoid purge valve was located at stack outlet. The anode side of the stack

was fed with pure hydrogen from the hydride-based tank. The pressure was reduced by a mechanical pressure regulator down to 50 mbar, which is the required pressure for the stack anode. The hydrogen mass flow and pressure were monitored at stack inlet. The anode purging strategy was implemented combining time and charge criteria. The maximum charge between purges was set to 500 C according to the fuel cell stack specifications. To ensure sufficient purging also at low stack power, the maximum time between purges was set to 20s. The purge period (time of valve open) was set to 0.05s. During startup, the purge valve was kept open for 5s after opening the hydrogen supply valve to flush out any extraneous gases from the anodic compartment.

The thermal coupling between the storage system and the stack was realized by a liquid external circuit, adopting trietylenglycol (TEG) as heat transfer medium. The electronic control of the APU was based on a National Instruments compact RIO control unit, implementing the required logics (start-up and shutdown procedures, normal operation, alarms and errors) coded using the Labview programming language. The scheme of the APU is reported in *Figure 6*. To facilitate and fasten the start-up of the APU, a small cylinder of compressed hydrogen (not shown in the scheme of *Figure 6*) was connected in parallel to the solid-state hydrogen storage system.

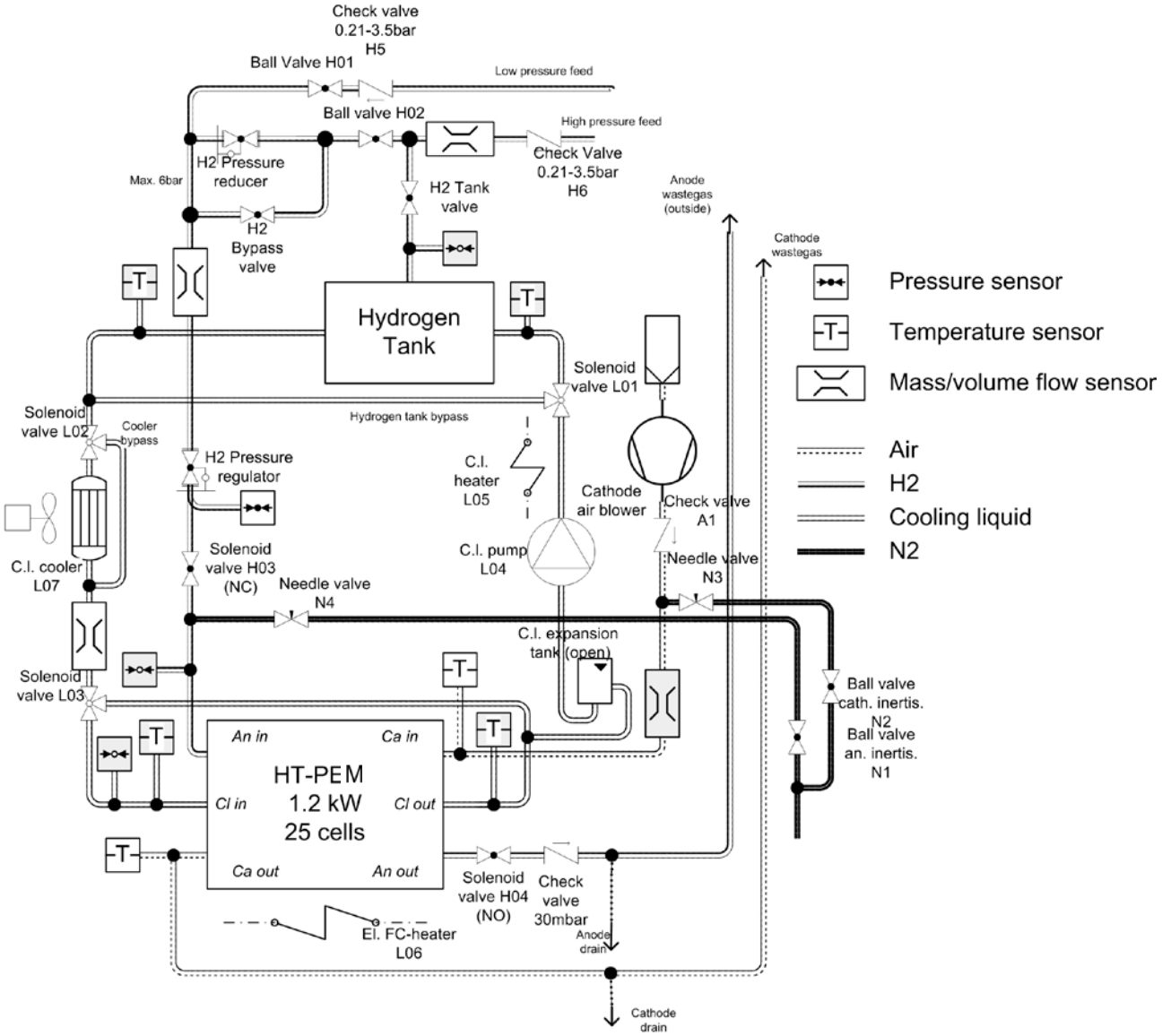


*Figure 6: Scheme of the APU. The hydrogen storage tank, the HT-PEM and the main auxiliary components are reported.*

### 3.4 APU installation and testing

After the integration of the hydrogen storage and fuel cell systems described in section 3.3, the APU was installed on an IVECO Daily Electric for the final road testing (see *Figure 7*). The APU was connected to the 12 V circuit of the vehicle to recharge the service batteries. The performances of the APU were measured on a real road scenario, defined coherently with the typical urban mission of selected type of vehicle. A custom urban cycle was defined with an average required power of 400 W and a current set point of 50 A.

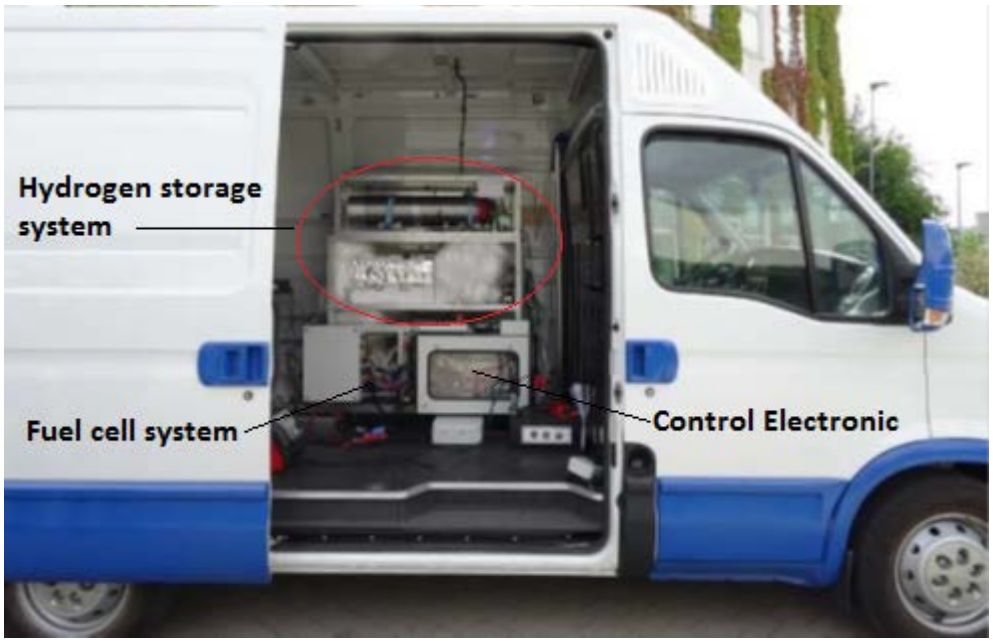


*Figure 7: APU installed on the IVECO Daily for the road testing.*

The total duration of the test was 4500 s. The starting temperatures of the fuel cell stack, heat transfer fluid and hydrogen storage material were 120 °C. *Figure 8* shows the time evolution of the electrical current (top), the temperature of the heat transfer fluid (middle) and of the storage system (bottom) during the test. The system required, using electric heating, 3100 s to reach 160 °C and for the remaining part of the test the thermal balance was assured by the heat generated by the fuel cell stack. The maximum gross current generated by the fuel cell stack was 45 A, and it remained constant for the whole duration of the test. The temperature distribution in the whole system was rather homogenous during the test, confirming the optimized running of the whole system.

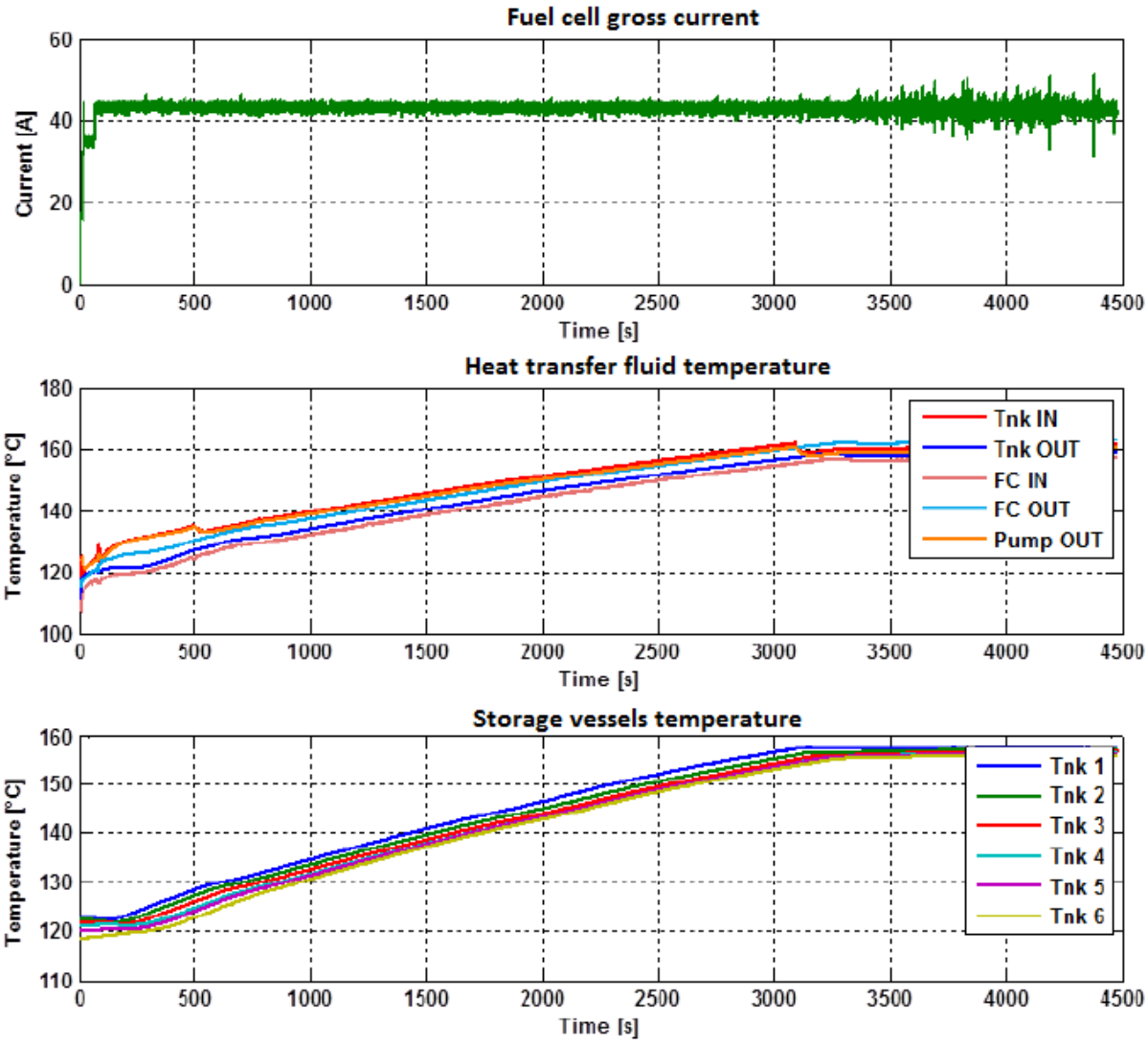


*Figure 8: Top: current generated by the fuel cell stack during the test. Middle: temperature of the heat transfer fluid in different points of the APU (storage system- Tnk = complete tank - inlet/outlet, FC = fuel cell inlet/outlet, Pump = circulating pump outlet). Bottom: temperatures of six of the twelve storage vessels (indicated with Tnk = single tanks).*

## 4 Conclusions

In this work, the development of a HT-PEM fuel cell APU with solid state hydrogen storage system was presented. A solid state hydrogen storage system with gravimetric capacity of 2.1%, fully reversible at 160-180 °C, was demonstrated. The combination of the mixed lithium amide/magnesium hydride system with a metal hydride to exploit the advantages of both materials was implemented. The auxiliary power unit was built integrating and thermally coupling the storage

system with a high temperature proton exchange membrane fuel cells stack. The APU was installed on a light duty commercial vehicle (IVECO Daily) and its performances were validated in an urban cycle in conditions similar to those found in real life applications.

As a result of the SSH2S project, it has been demonstrated for the first time that a hydrogen tank based on complex hydrides can be suitably used to feed a HT-PEM fuel cell, powering a 1 kW APU. For possible commercial implementation of the developed prototype, an increase of the power up to 5 kW should be considered. In addition, an optimization of the design might reduce the total weight of the system, possibly leading to performances comparable to existing APU based on fuel cells using compressed gas hydrogen storage.

**Acknowledgments**

The research leading to these results has received funding from the European Union's Seventh Framework Programme (FP7/2007-2013) for the Fuel Cells and Hydrogen Joint Technology Initiative under grant agreement n. 256653.

Elisa Albanese, Serena Ballarin, Marek Bielewski, Silvia Bordiga, Inga Buerger, Valerio Calò, Bartolomeo Civalleri, Alessandro De Filippo, Stefano Deledda, Francesco Dolci, Paolo Florian, Massimo Fossanetti, Jianjiang Hu, Georgios Kalantzopoulos, Jiri Muller, Eugenio Pinatel, Giuseppe Spoto, Ulrich Ulmer, Jenny Vitillo and Jörg Weiss-Ungethüm are acknowledged for their contribution to the SSH2S project.

**References**

[1] SSH2S European research project, (2015). www.ssh2s.eu.

[2] J. Lawrence, M. Boltze, Auxiliary power unit based on a solid oxide fuel cell and fuelled with diesel, J. Power Sources. 154 (2006) 479–488. doi:10.1016/j.jpowsour.2005.10.036.

[3] P. Nehter, J.B. Hansen, P.K. Larsen, A techno-economic comparison of fuel processors utilizing diesel for solid oxide fuel cell auxiliary power units, J. Power Sources. 196 (2011) 7347–7354. doi:10.1016/j.jpowsour.2010.09.011.

[4] S. Jain, H.-Y. Chen, J. Schwank, Techno-economic analysis of fuel cell auxiliary power units as alternative to idling, J. Power Sources. 160 (2006) 474–484. doi:10.1016/j.jpowsour.2006.01.083.

[5] F. Baratto, U.M. Diwekar, D. Manca, Impacts assessment and trade-offs of fuel cell-based auxiliary power units Part I: System performance and cost modeling, J. Power Sources. 139 (2005) 205–213. doi:10.1016/j.jpowsour.2004.07.023.

[6] F. Baratto, U.M. Diwekar, D. Manca, Impacts assessment and tradeoffs of fuel cell based auxiliary power units Part II. Environmental and health impacts, LCA, and multi-objective optimization, J. Power Sources. 139 (2005) 214–222. doi:10.1016/j.jpowsour.2004.07.024.

[7] S. Specchia, F.W.A. Tillemans, P.F. Van Den Oosterkamp, G. Saracco, Conceptual design and selection of a biodiesel fuel processor for a vehicle fuel cell auxiliary power unit, J. Power Sources. 145 (2005) 683–690. doi:10.1016/j.jpowsour.2004.12.076.

[8] M. Sgroi, G. Bollito, G. Saracco, S. Specchia, BIOFEAT: Biodiesel fuel processor for a vehicle fuel cell auxiliary power unit: Study of the feed system, J. Power Sources. 149 (2005) 8–14. doi:10.1016/j.jpowsour.2004.12.059.

[9] J. Karstedt, J. Ogrzewalla, C. Severin, S. Pischinger, Development and design of experiments optimization of a high temperature proton exchange membrane fuel cell auxiliary power unit with onboard fuel processor, J. Power Sources. 196 (2011) 9998–10009.

doi:10.1016/j.jpowsour.2011.07.034.

[10] Y. Liu, W. Lehnert, H. Janßen, R.C. Samsun, D. Stolten, A review of high-temperature polymer electrolyte membrane fuel-cell (HT-PEMFC)-based auxiliary power units for diesel-powered road vehicles, J. Power Sources. 311 (2016) 91–102. doi:10.1016/j.jpowsour.2016.02.033.

[11] G. Doucet, C. Etiévant, C. Puyenchet, S. Grigoriev, P. Millet, Hydrogen-based PEM auxiliary power unit, Int. J. Hydrogen Energy. 34 (2009) 4983–4989. doi:10.1016/j.ijhydene.2008.12.029.

[12] R. Urbanczyk, S. Peil, D. Bathen, C. Heßke, J. Burfeind, K. Hauschild, M. Felderhoff, F. Schüth, HT-PEM fuel cell system with integrated complex metal hydride storage tank, in: Fuel Cells, WILEY-VCH Verlag, 2011: pp. 911–920. doi:10.1002/fuce.201100012.

[13] B. Delhomme, A. Lanzini, G.A. Ortigoza-Villalba, S. Nachev, P. De Rango, M. Santarelli, P. Marty, P. Leone, Coupling and thermal integration of a solid oxide fuel cell with a magnesium hydride tank, Int. J. Hydrogen Energy. 38 (2013) 4740–4747. doi:10.1016/j.ijhydene.2013.01.140.

[14] C. Song, L.E. Klebanoff, T.A. Johnson, B.S. Chao, A.F. Socha, J.M. Oros, C.J. Radley, S. Wingert, J.S. Breit, Using metal hydride H2 storage in mobile fuel cell equipment: Design and predicted performance of a metal hydride fuel cell mobile light, Int. J. Hydrogen Energy. 39 (2014) 14896–14911. doi:10.1016/j.ijhydene.2014.07.069.

[15] M. V. Lototskyy, I. Tolj, A. Parsons, F. Smith, C. Sita, V. Linkov, Performance of electric forklift with low-temperature polymer exchange membrane fuel cell power module and metal hydride hydrogen storage extension tank, J. Power Sources. 316 (2016) 239–250. doi:10.1016/j.jpowsour.2016.03.058.

[16] M.B. Ley, L.H. Jepsen, Y.S. Lee, Y.W. Cho, J.M. Bellosta Von Colbe, M. Dornheim, M. Rokni, J.O. Jensen, M. Sloth, Y. Filinchuk, J.E. Jørgensen, F. Besenbacher, T.R. Jensen,

Complex hydrides for hydrogen storage - New perspectives, Mater. Today. 17 (2014) 122–128. doi:10.1016/j.mattod.2014.02.013.

[17] S. Orimo, Y. Nakamori, J.R. Eliseo, A. Züttel, C.M. Jensen, Complex hydrides for hydrogen storage., Chem. Rev. 107 (2007) 4111–4132. doi:10.1021/cr0501846.

[18] E. Callini, Z.Ö.K. Atakli, B.C. Hauback, S. ichi Orimo, C. Jensen, M. Dornheim, D. Grant, Y.W. Cho, P. Chen, B. Hjörvarsson, P. de Jongh, C. Weidenthaler, M. Baricco, M. Paskevicius, T.R. Jensen, M.E. Bowden, T.S. Autrey, A. Züttel, Complex and liquid hydrides for energy storage, Appl. Phys. A Mater. Sci. Process. 122 (2016) 353. doi:10.1007/s00339-016-9881-5.

[19] P. Pfeifer, C. Wall, O. Jensen, H. Hahn, M. Fichtner, Thermal coupling of a high temperature PEM fuel cell with a complex hydride tank, Int. J. Hydrogen Energy. 34 (2009) 3457–3466. doi:10.1016/j.ijhydene.2009.02.041.

[20] Z. Xiong, G. Wu, J. Hu, P. Chen, Ternary imides for hydrogen storage, Adv. Mater. 16 (2004) 1522–1525. doi:10.1002/adma.200400571.

[21] P. Chen, Z. Xiong, G. Wu, Y. Liu, J. Hu, W. Luo, Metal-N-H systems for the hydrogen storage, Scr. Mater. 56 (2007) 817–822. doi:10.1016/j.scriptamat.2007.01.001.

[22] W. Luo, E. Rönnebro, Towards a viable hydrogen storage system for transportation application, J. Alloys Compd. 404–406 (2005) 392–395. doi:10.1016/j.jallcom.2005.01.131.

[23] W. Lohstroh, M. Fichtner, Reaction steps in the Li-Mg-N-H hydrogen storage system, J. Alloys Compd. 446–447 (2007) 332–335. doi:10.1016/j.jallcom.2006.12.060.

[24] J. Hu, A. Pohl, S. Wang, J. Rothe, M. Fichtner, Additive effects of LiBH4 and ZrCoH3 on the hydrogen sorption of the Li-Mg-N-H hydrogen storage system, J. Phys. Chem. C. 116 (2012) 20246–20253. doi:10.1021/jp307775d.

[25] U. Ulmer, J. Hu, M. Franzreb, M. Fichtner, Preparation, scale-up and testing of nanoscale, doped amide systems for hydrogen storage, Int. J. Hydrogen Energy. 38 (2013) 1439–1449.

doi:10.1016/j.ijhydene.2012.10.115.

[26] X. Zhang, Z. Li, F. Lv, H. Li, J. Mi, S. Wang, X. Liu, L. Jiang, Improved hydrogen storage performance of the LiNH2-MgH2-LiBH4 system by addition of ZrCo hydride, Int. J. Hydrogen Energy. 35 (2010) 7809–7814. doi:10.1016/j.ijhydene.2010.05.095.

[27] M. Bielewski, E. Napolitano, J. Vitillo, M. Baricco, A. Masala, M. Fichtner, J. Hu, Comparison of the material degradation rate measurements using different approaches on example of Li-Mg-N-H system, in: 15th Int. Symp. Met. Syst. 7-12 August, Interlaken, Switzerland., 2016.

[28] O.C. Zienkiewicz, R.L. Taylor, J.Z. Zhu, The Finite Element Method Set, 7th ed., Butterworth Heinemann, 2005. doi:10.1016/B978-075066431-8.50194-6.

[29] Comsol Multyphysics, (2016). https://www.comsol.com/.

[30] I. Bürger, J.J. Hu, J.G. Vitillo, G.N. Kalantzopoulos, S. Deledda, M. Fichtner, M. Baricco, M. Linder, Material properties and empirical rate equations for hydrogen sorption reactions in 2 LiNH2-1.1-MgH2-0.1-LiBH4-3 wt.% ZrCoH3, Int. J. Hydrogen Energy. 39 (2014) 8283–8292. doi:10.1016/j.ijhydene.2014.02.120.

[31] J. Hu, A. Pohl, S. Wang, J. Rothe, M. Fichtner, Additive effects of LiBH4 and ZrCoH3 on the hydrogen sorption of the Li-Mg-N-H hydrogen storage system, J. Phys. Chem. C. 116 (2012) 20246–20253. doi:10.1021/jp307775d.

[32] I. Bürger, M. Bhouri, M. Linder, Considerations on the H2 desorption process for a combination reactor based on metal and complex hydrides, Int. J. Hydrogen Energy. 40 (2015) 7072–7082. doi:10.1016/j.ijhydene.2015.03.136.

[33] M. Bhouri, I. Bürger, M. Linder, Optimization of hydrogen charging process parameters for an advanced complex hydride reactor concept, Int. J. Hydrogen Energy. 39 (2014) 17726–17739. doi:10.1016/j.ijhydene.2014.08.100.

[34] M. Bhouri, I. Bürger, M. Linder, Numerical investigation of hydrogen charging performance

for a combination reactor with embedded metal hydride and coolant tubes, Int. J. Hydrogen Energy. 40 (2015) 6626–6638. doi:10.1016/j.ijhydene.2015.03.060.

[35] M. Klell, Storage of Hydrogen in the Pure Form, in: Michael Hirscher (Ed.), Handb. Hydrog. Storage, WILEY-VCH, 2010: pp. 1–38.

Figure(s) - provide separately in addition to within the manuscript file
Click here to download high resolution image

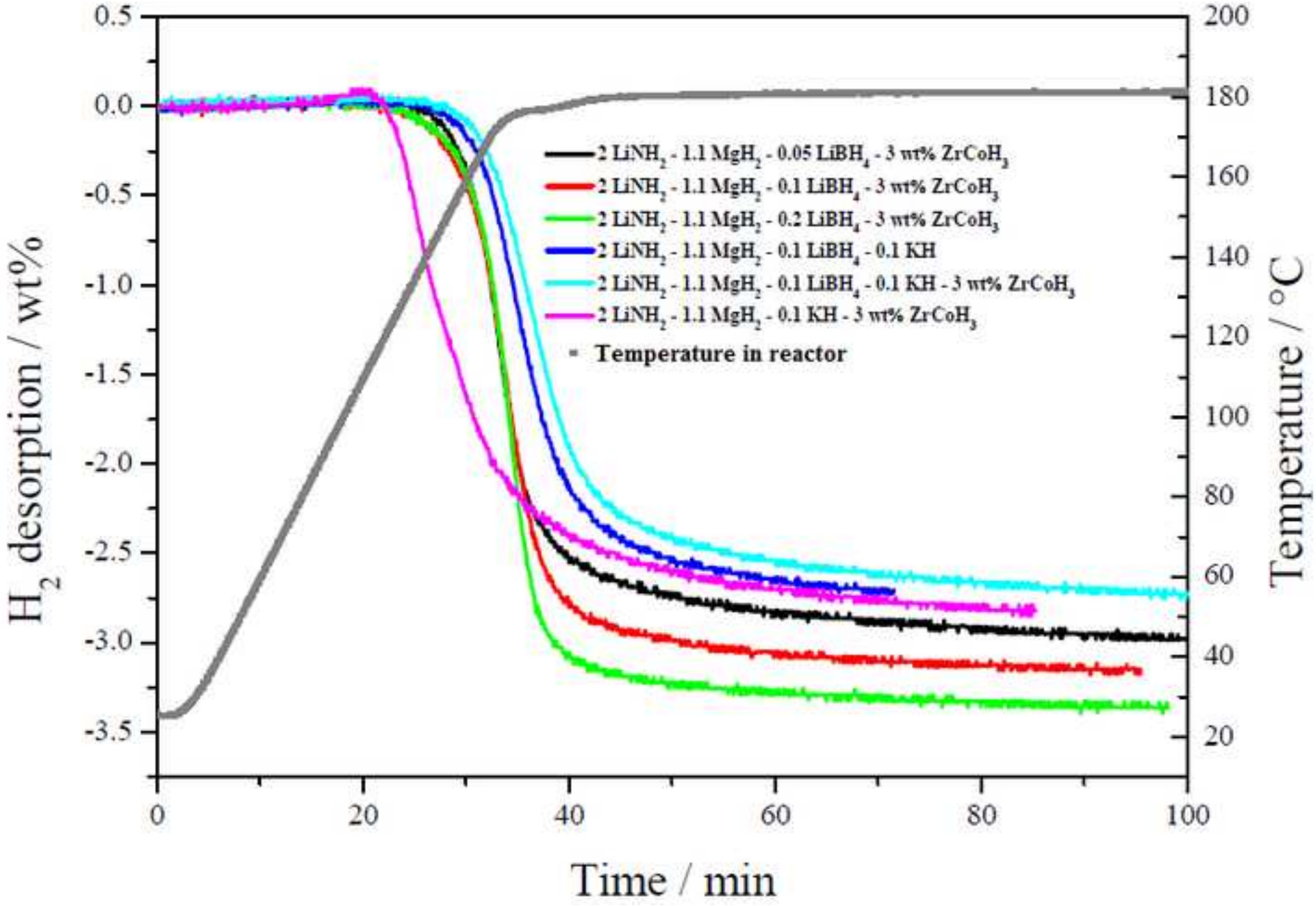

**Figure(s) - provide separately in addition to within the manuscript file**
**Click here to download high resolution image**

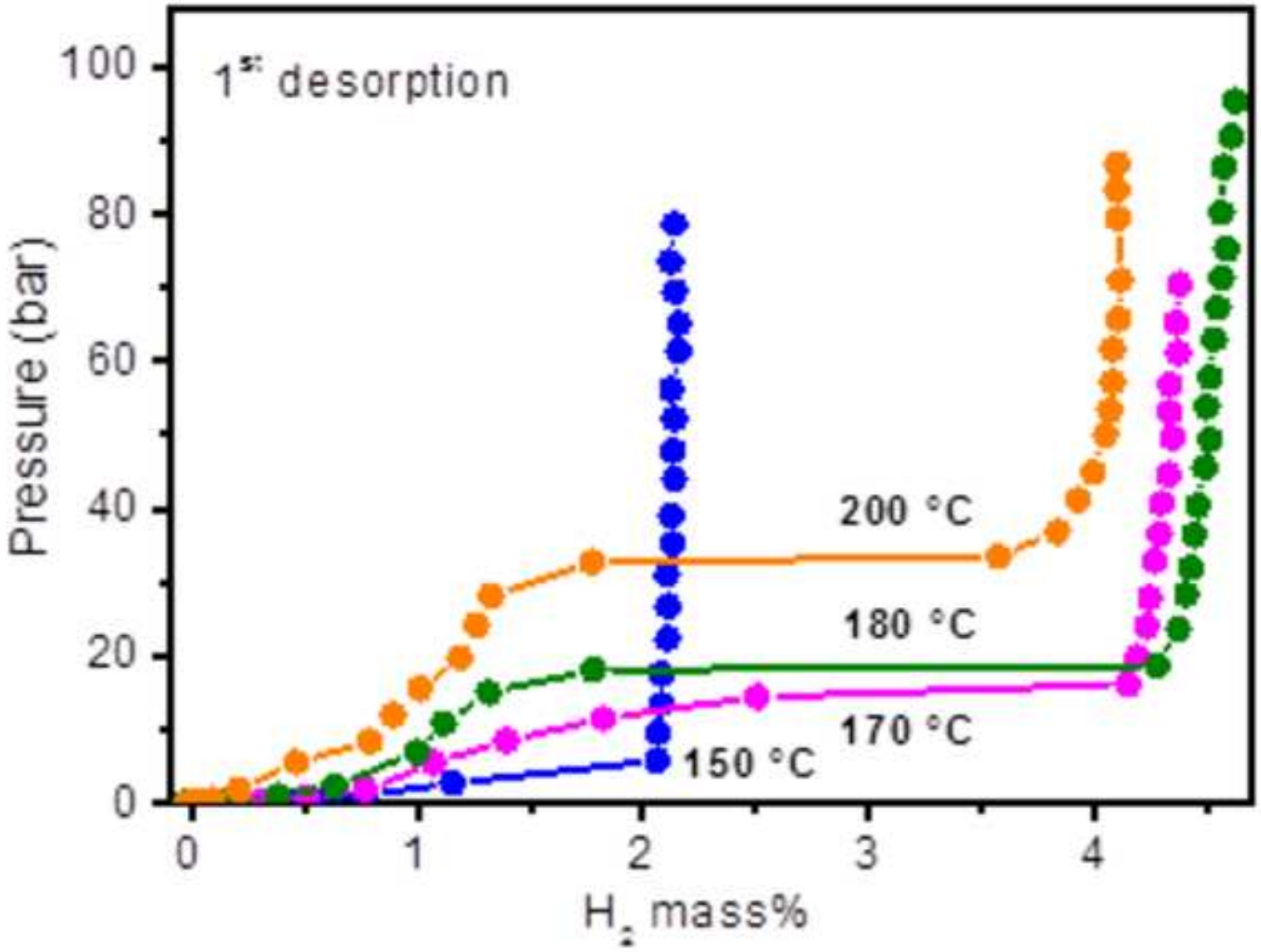

**Figure(s) - provide separately in addition to within the manuscript file**
**Click here to download high resolution image**

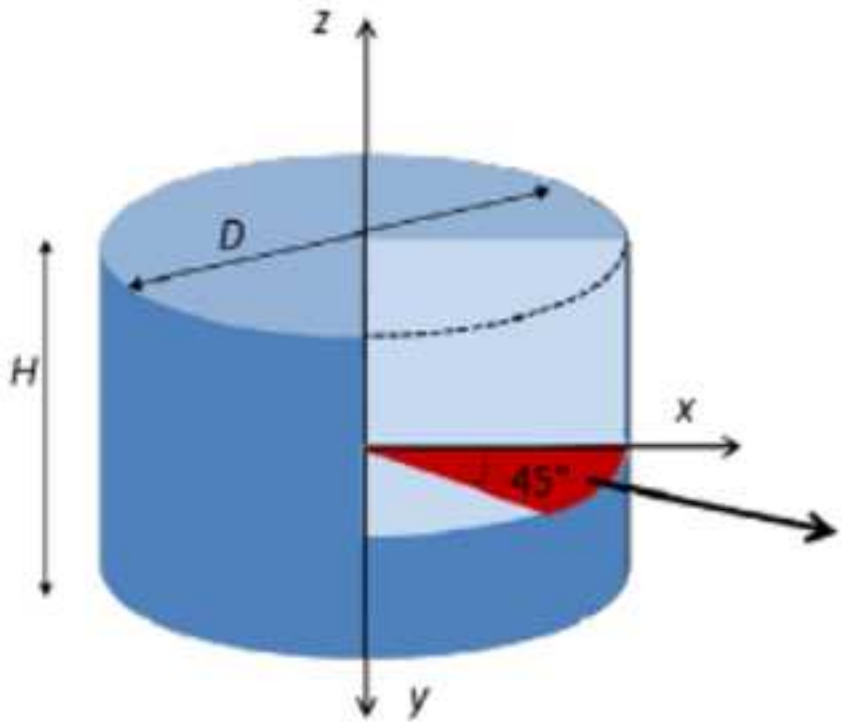


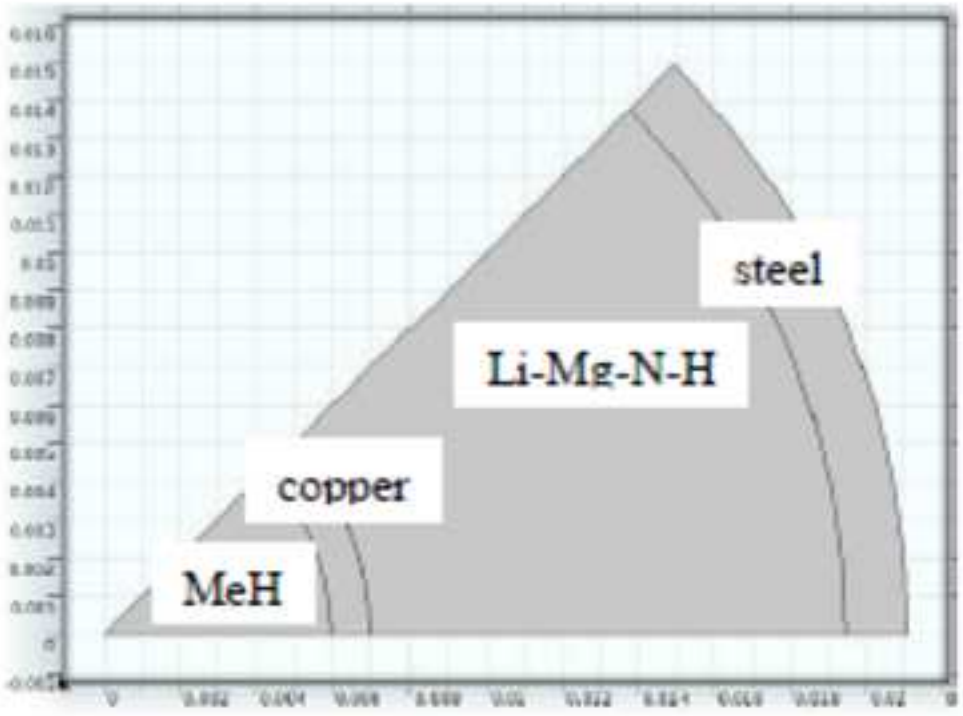

**Figure(s) - provide separately in addition to within the manuscript file**
**Click here to download high resolution image**

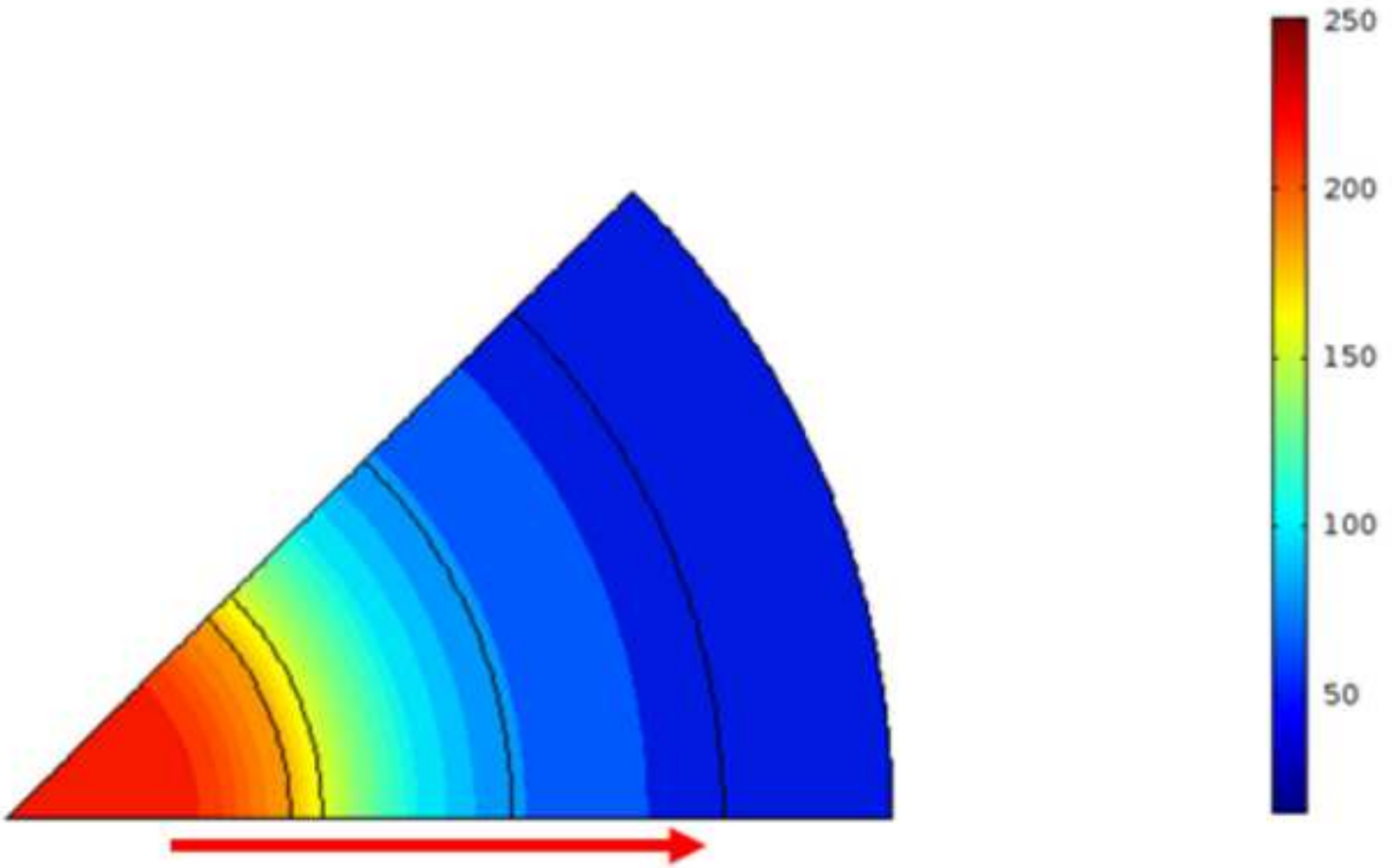

Figure(s) - provide separately in addition to within the manuscript file
Click here to download high resolution image

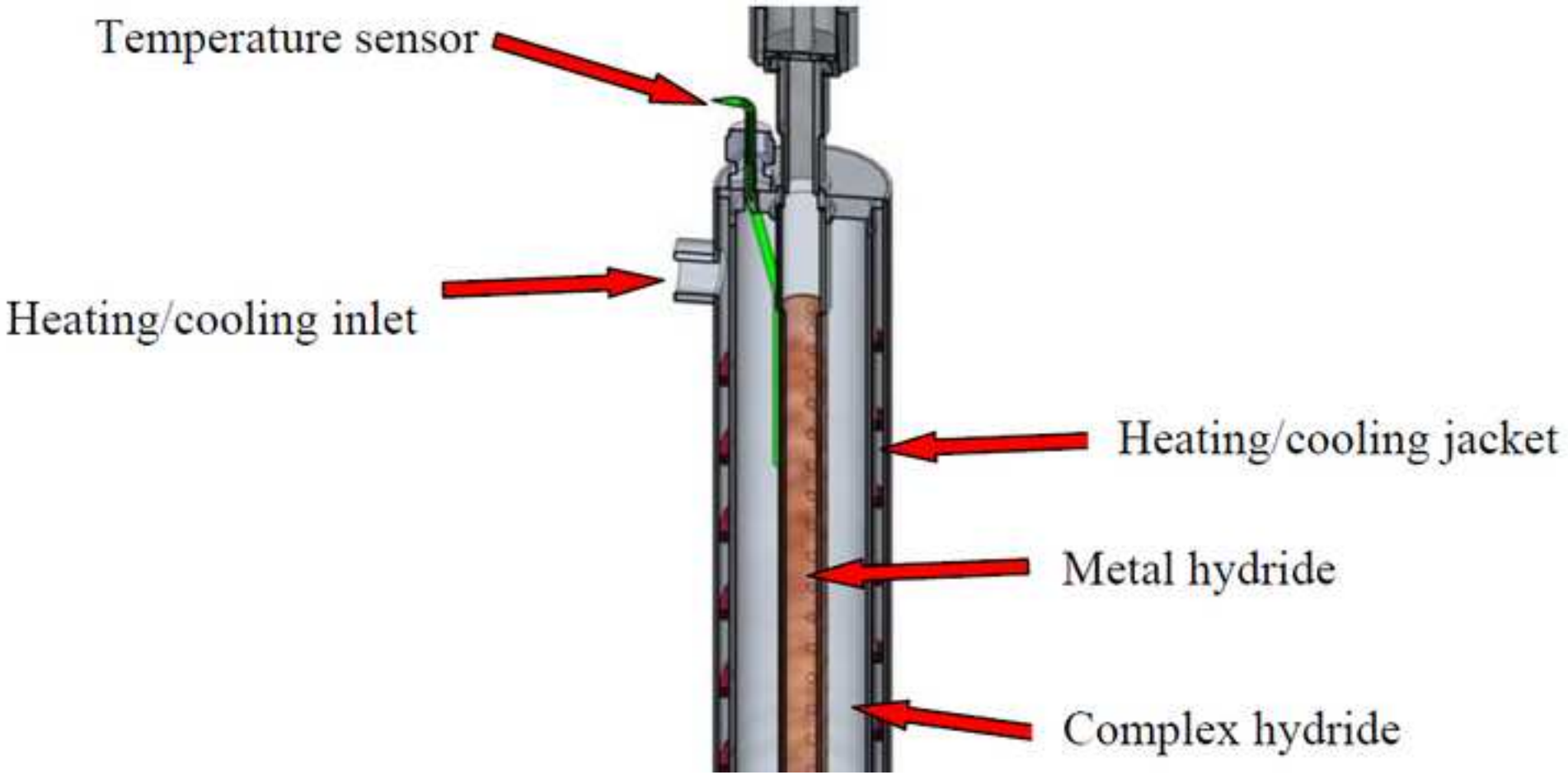

**Figure(s) - provide separately in addition to within the manuscript file**
**Click here to download high resolution image**

**Figure(s) - provide separately in addition to within the manuscript file**
**Click here to download high resolution image**

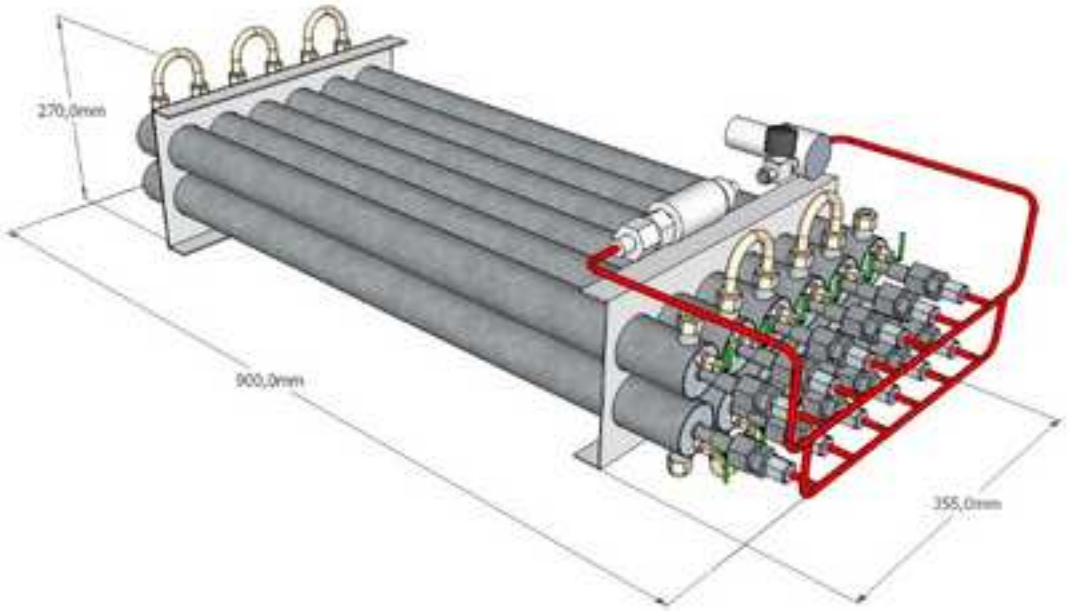

**Figure(s) - provide separately in addition to within the manuscript file**
**Click here to download high resolution image**

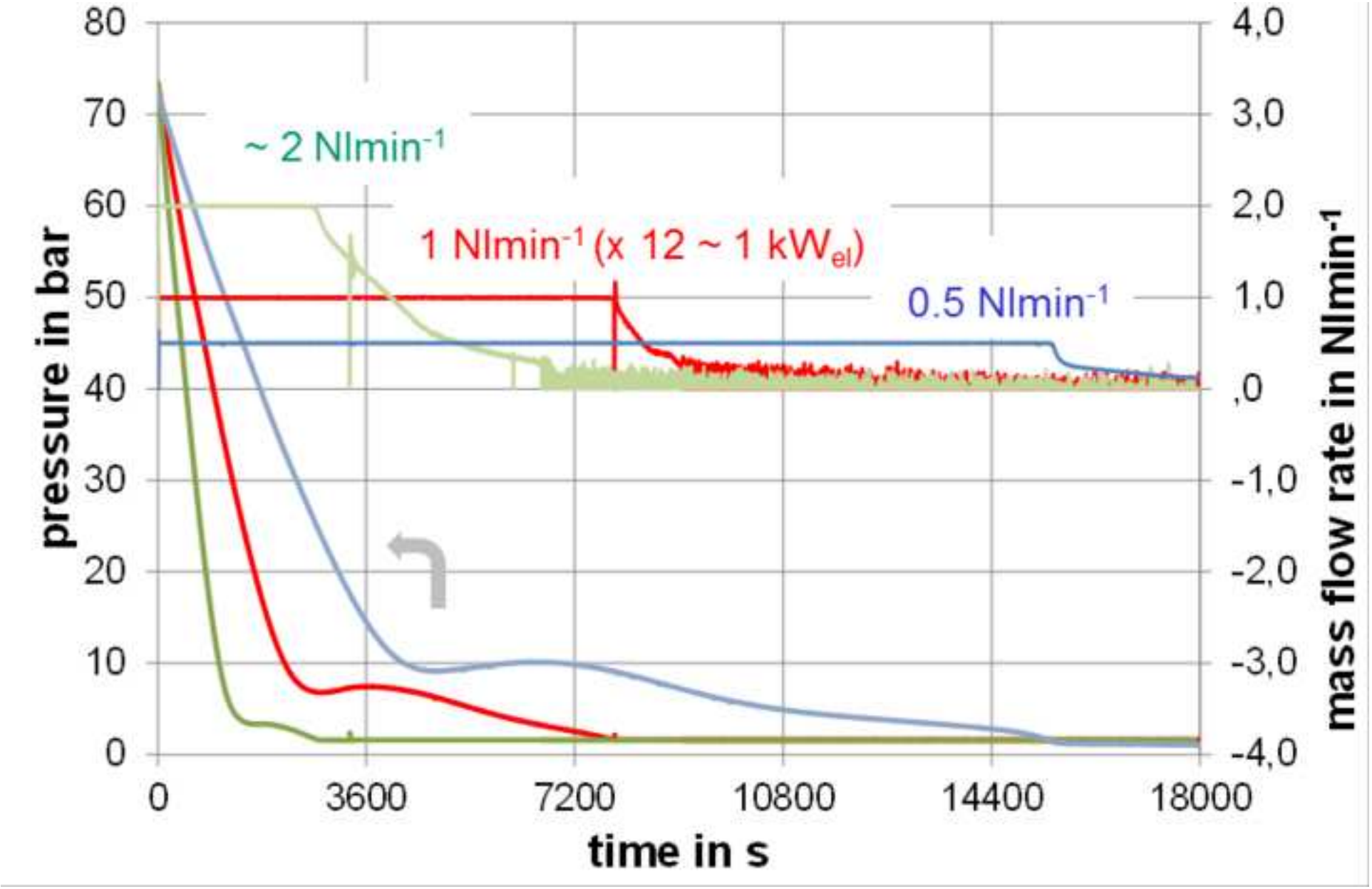

**Figure(s) - provide separately in addition to within the manuscript file**
**Click here to download high resolution image**

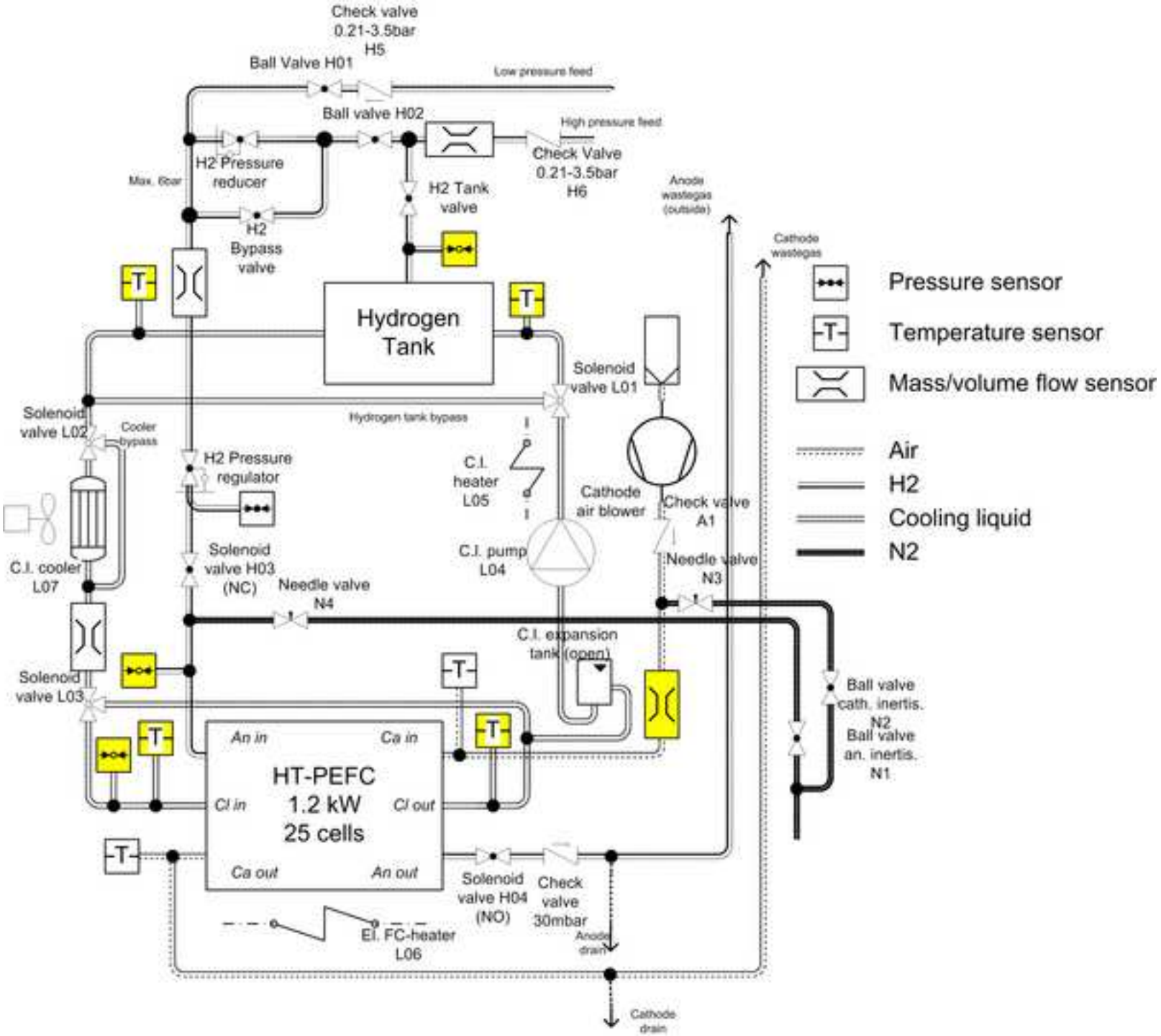

**Figure(s) - provide separately in addition to within the manuscript file**
**Click here to download high resolution image**

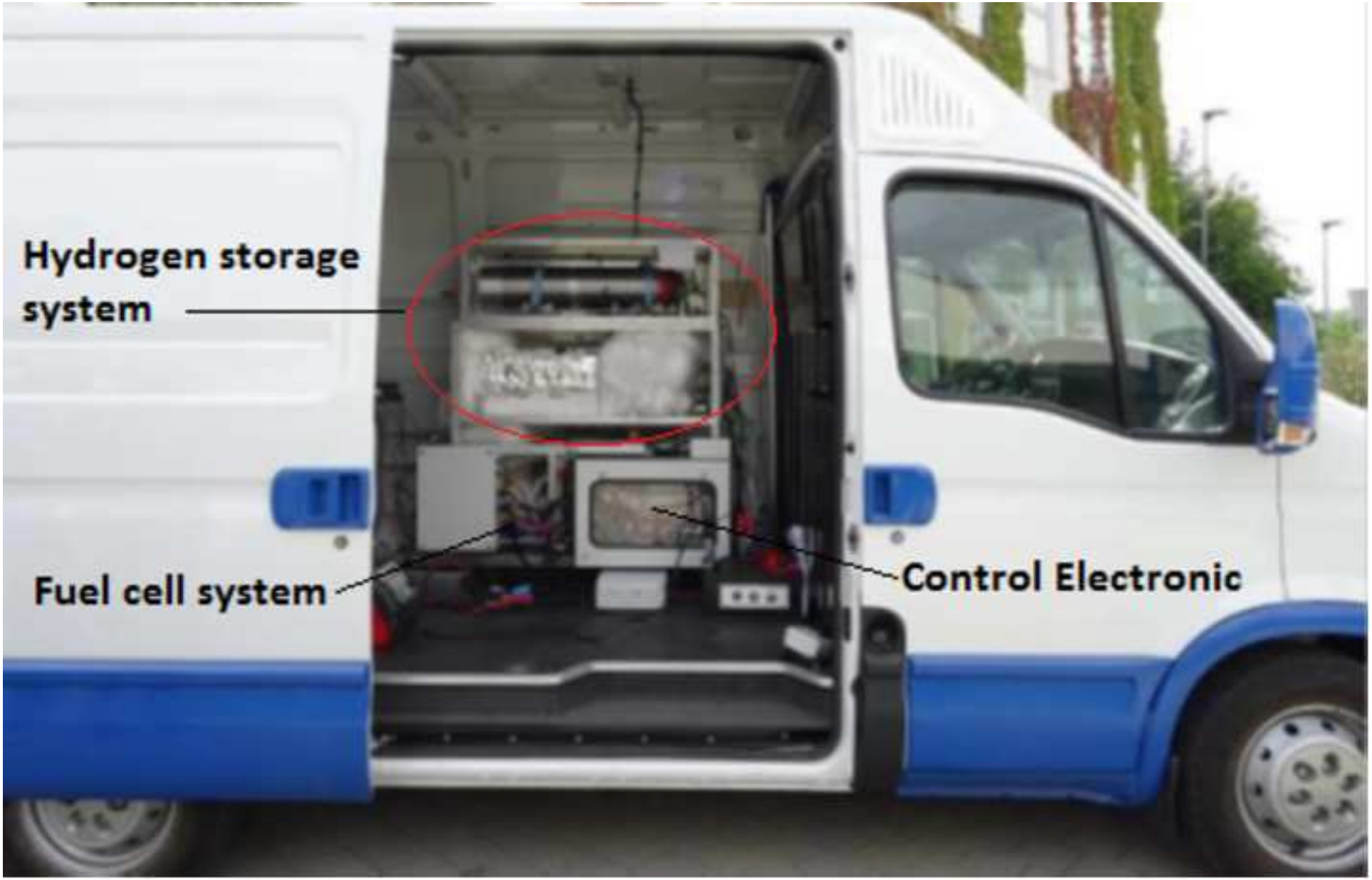

**Figure(s) - provide separately in addition to within the manuscript file**
**Click here to download high resolution image**

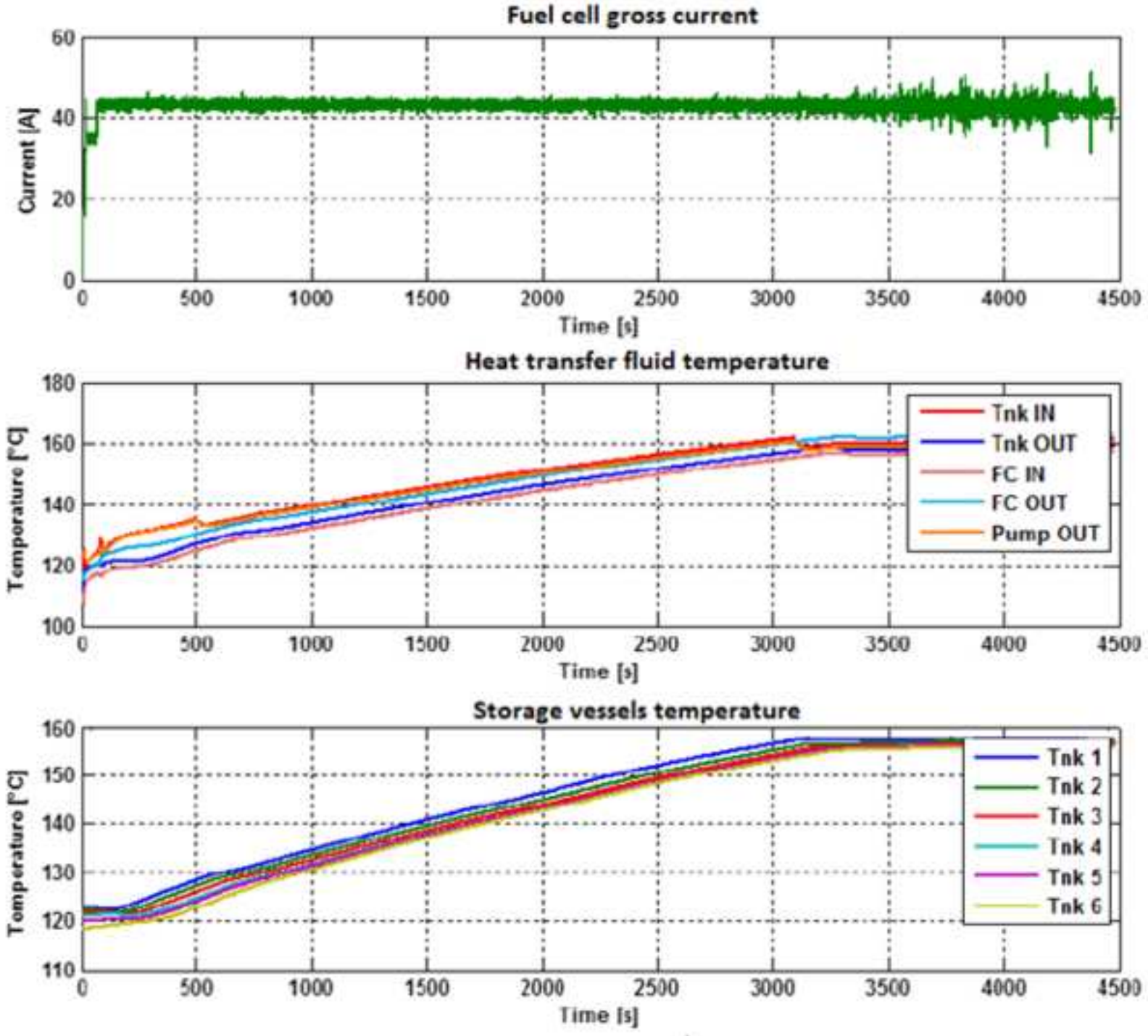

**Captions for "SSH2S: auxiliary power unit based on complex hydrides and high temperature polymeric fuel cells"**

*Figure 1: Hydrogen desorption isotherms under 0.1 MPa of hydrogen for the 2 $LiNH_2$ – 1.1 $MgH_2$ systems with and without addition of $LiBH_4$, $ZrCoH_3$ or KH in varying amounts.*

*Figure 2: PCI curves ($2^{nd}$ desorption, after activation) of the 2$LiNH_2$ - 1.1$MgH_2$ - 0.1$LiBH_4$ - 3wt%$ZrCoH_3$ system at 150 °C (squares), 170 °C (diamond), 180 °C (triangles) and 200 °C (circles).*

*Figure 3: Left and middle: tank geometry used for simulation. Right: results of 2D simulation at the point in time shortly before the CxH starts to absorb and increases its temperature. The red arrow indicates the direction of heat flux. The bar indicated the temperature scale.*

*Figure 4: a) Scheme of single vessel implementing the double storage materials concept (combi-tank); b) assembly of twelve vessels in parallel to form the complete storage system; c) overall dimensions of the system.*

*Figure 5: Hydrogen desorption from one single tube at 180 °C. Flow rates (right side) and corresponding pressure (left side) are shown as a function of time. Final tank consists of 12 similar tubes operated in parallel.*

*Figure 6: Scheme of the APU. The hydrogen storage tank, the HT-PEM and the main auxiliary components are reported.*

*Figure 7: APU installed on the IVECO Daily for the road testing.*

*Figure 8: Top: current generated by the fuel cell stack during the test. Middle: temperature of the heat transfer fluid in different points of the APU (storage system- Tnk=complete tank - inlet/outlet, fuel cell inlet/outlet, circulating pump outlet). Bottom: temperatures of six of the twelve storage vessels (indicated with Tnk=single tanks).*

*Table 1: Specifications of the 1kW APU.*